

Commensurability oscillations of rectangular antidot arrays: A classical diffusion model

J. Rychen, T. Vančura, and T. Heinzel

Solid State Physics Laboratory, ETH Zürich, CH-8093 Zürich, Switzerland

R. Schuster

Sektion Physik, LMU München, 80539 München, Germany

K. Ensslin

*Solid State Physics Laboratory, ETH Zürich, CH-8093 Zürich, Switzerland
and Sektion Physik, LMU München, 80539 München, Germany*

(Received 6 February 1998)

We have studied magnetoresistivity oscillations in rectangular lateral antidot superlattices both in low-temperature electron transport experiments as well as in a classical diffusion model. Within this model, the conductivity tensor is obtained from a numerical simulation of the spatial distribution of electrons diffusing in the antidot array. It is demonstrated that all the essential features of the measured magnetoconductivity can be reproduced within this classical model. Maps of the trajectories in real space give an intuitive understanding of the mechanism that causes the anisotropies in the conductivity. [S0163-1829(98)06028-7]

I. INTRODUCTION

Magnetotransport experiments on antidot lattices in two-dimensional electron gases have revealed a variety of unpredicted features.¹ Characteristic magnetoresistivity oscillations²⁻⁴ in square antidot lattices have been observed experimentally and explained by numerical simulations⁵ based on the classical equation of motion and Kubo's linear response theory.⁶ Basically the maxima in the magnetoresistance are thought to arise from either pinned orbits around groups of antidots³⁻⁵ or from so-called runaway trajectories,⁷⁻⁹ electrons bouncing from antidot to antidot. The numerical simulations of the magnetoresistance are in excellent agreement with experimental results.^{5,10,11} Nevertheless, the influence of the significant types of orbits strongly depends on the details of the samples. In this paper, classical trajectories are calculated building on methods developed and used by other authors.⁵ However, for the interpretation we do not concentrate on Poincaré sections in phase space but rather on diffusion clouds in real space, similar as it has been done by Lorke, Kotthaus, and Ploog⁴ for square lattices. We demonstrate that numerical simulations of the classical electron diffusion can explain the magnetotransport in rectangular antidot arrays^{10,12-15} to a surprisingly large extent. The pictures of typical trajectories nicely illustrate the origin of the magnetic-field-dependent anisotropy of the conductivity.

The outline of the paper is as follows: In Sec. II, we describe our experimental setup for the low-temperature transport experiments. In Sec. III, our numerical model is introduced. The experimental and numerical results are compared in Sec. IV. We conclude with a summary and an outlook.

II. EXPERIMENT

To study anisotropy effects in rectangular antidot lattices, we defined antidots in a two-dimensional electron gas

(2DEG) of a Ga[Al]As heterostructure with a sheet density $n_{2d} = 3.5 \times 10^{16} \text{ m}^{-2}$ and a mobility of $\mu = 76 \text{ m}^2/\text{V s}$. In order to measure all four components of the $2d$ -resistivity tensor, the sample was processed to an L-shaped Hall bar [Fig. 1(a)]. A rectangular antidot lattice with periods of $a_x = 240 \text{ nm}$ and $a_y = 480 \text{ nm}$ aligned to the Hall bars were defined by electron beam lithography followed by wet chemical etching. To keep the lateral depletion minimal, only the cap layer and a part of the Si-doped layer have been removed. The resulting potential landscape has relatively steep sidewalls and weak saddle points between two antidots [see the modeled potential landscape in Fig. 1(b)]. Further details of this sample are described in Ref. 16. The components of the magnetoresistivity tensor have been measured at low temperatures ($T = 1.7 \text{ K}$) and in magnetic fields up to 8 T perpendicular to the plane of the electron gas. For high magnetic fields ($B > 2 \text{ T}$), Shubnikov-de Haas oscillations and the quantum Hall effect occur as in an unpatterned 2DEG and give the possibility to determine the electron sheet density n_{2d} . At lower magnetic fields ($B < 2 \text{ T}$),

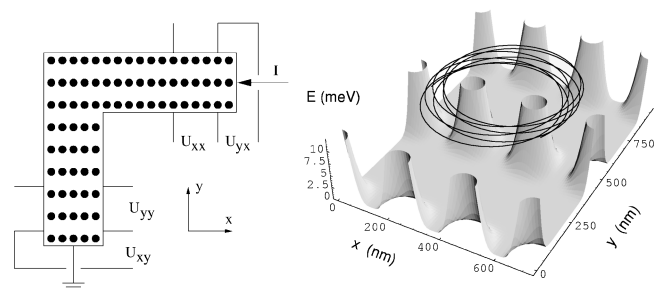


FIG. 1. Left: L-shaped Hall bar to measure all the components of the resistivity tensor. Right: The potential landscape of the antidots used for the simulations. The radius of the antidots at the Fermi energy is $r = 0.18a_x$ and the steepness parameter is $\beta = 2$. The shown trajectory is for a magnetic field where the cyclotron diameter $2R_c = 2a_x$ ($B = 0.42 \text{ T}$).

anomalous peaks in the longitudinal resistivity ρ_{ii} are observed, especially for the current direction perpendicular to the antidot rows (the y direction in Fig. 1(a)). For these peaks the classical cyclotron radius

$$R_c = \frac{m^* v_F}{eB} \quad (1)$$

is an integer multiple of the lattice constant. Here, m^* is the effective electron mass, v_F the Fermi velocity. The conductivity tensor σ_{ij} is computed from the experimental data by inverting the resistivity tensor ρ_{ij} . It was shown theoretically¹⁰ and experimentally¹⁷ that the conductivity through the rows of antidots σ_{yy} is predominately related to the resistivity ρ_{xx} obtained from current flow along the antidot rows and vice versa. Care was taken to perform all measurements at equal electron densities in both arms of the L-shaped Hall bar.

III. NUMERICAL SIMULATIONS

A. Trajectories

The potential $V(x,y)$ of the rectangular antidot lattice is modeled by

$$V(x,y) = V_0 \left(\cos^2 \frac{\pi}{a_x} x \right)^\beta \left(\cos^2 \frac{\pi}{a_y} y \right)^{\beta\gamma}, \quad (2)$$

where V_0 is the amplitude of the potential modulation, chosen such that the size of the antidots in the x direction at the Fermi energy is of given radius r : $V_0 = E_F / [\cos^2(r\pi/a_x)]^\beta$. The parameter β determines the steepness of the antidot potential and $\gamma = \ln(E_F/V_0) / [\beta \ln \cos^2(r\pi/a_y)]$ is adjusted to obtain circular antidots at the Fermi energy. It has, however, been argued that the antidots are not circular because the screening is expected to be weaker between neighboring antidots.¹⁶ The potential landscape is described by two parameters, namely, r and β . The equation of motion for an electron in this potential and a perpendicular magnetic field B has been solved numerically as described in Ref. 5.

In our simulations, an electron scatters after a time τ that is randomly chosen with the distribution for a mean scattering time τ_c

$$P[\tau=t] = \frac{1}{\tau_c} e^{-(t/\tau_c)}, \quad (3)$$

and it changes the direction of flight by a random angle. That means that the differential scattering rate $\tau^{-1}(\theta)$ as a function of the scatter angle θ is constant and so the quantum scattering time $\tau_q^{-1} = \int_{-\pi}^{\pi} \tau^{-1}(\theta) d\theta$ and the Drude scattering time $\tau_D^{-1} = \int_{-\pi}^{\pi} \tau^{-1}(\theta) (1 - \cos \theta) d\theta$ are the same in this model. Our sample is made of a wafer with a mobility of $\mu = 76 \text{ m}^2/\text{V s}$ corresponding to a Drude scattering time of $\tau_D = 30 \text{ ps}$. However, the intrinsic scattering time in the antidot sample is not exactly known. It is known that electron beam lithography can reduce the mobility and that at the borders of the antidots, where the electron density fades out and hence the screening is reduced, the intrinsic scattering is enhanced. In the simulations a scattering time of $\tau_c = 13.5 \text{ ps}$ is used, as this corresponds to a mean free path of $l_c \approx 14a_x$, based on best agreement with experimental data. In

conservative systems with two degrees of freedom the accessible phase space is the $3d$ energy surface Γ separated into disjoint parts Γ_i by invariant tori that can be investigated by Poincaré surfaces, for example, the sections (y, v_y) at $(x \bmod a_x = 0)$. In the absence of scattering events we can distinguish between invariant tori of chaotic orbits and regular orbits surrounding a group of antidots (for certain ranges of magnetic field). In Ref. 5 it has been argued that only the chaotic trajectories contribute to the conductivity because the regular orbits are pinned and do not drift away when an electric field is applied. Here, however, the impurity scattering is incorporated into the simulation of the trajectories and hence the whole accessible phase space gets connected: an electron can scatter from a chaotic orbit into a regular orbit and vice versa. We therefore do not distinguish between different parts of the phase space.

B. Calculation of the conductivity

It is straightforward to calculate numerically¹⁸ the conductivity tensor σ_{ij} , which is related to the diffusion tensor D_{ij} by the Einstein equation

$$\sigma_{ij} = e^2 D(E_F) D_{ij}, \quad (4)$$

with $D(E_F)$ being the density of states at the Fermi energy E_F . The diagonal components are obtained by a direct simulation of the diffusion process. The applied electrical field is not considered in the simulation because it is irrelevant in linear response approximation.⁶ The density of states is assumed to be unaffected by the antidots and the magnetic field. However, the quantum-mechanical miniband structure has been calculated¹⁹ and successfully applied to interpret the observation of quantum oscillations²⁰ on arrays with relatively large antidots. The solution for the diffusion problem in one dimension for n_0 particles starting at $x=0$, $t=0$ is

$$n(x,t) = \frac{n_0}{\sqrt{4\pi Dt}} e^{-(x^2/4Dt)}, \quad (5)$$

where D is the diffusion constant and $n(x,t)$ the density distribution for the observed electrons. We have calculated 1000 trajectories with starting points randomly distributed in the elementary cell $[0,a] \times [0,b]$ (except for the circle cut out by the antidots) and random direction of initial velocity for a time $t_s = 10\tau_c$ long. As mentioned above, the trajectories are not restricted on invariant tori but can reach the whole $3d$ energy surface and so the results do not depend on the initial distribution as long as the simulated time is long enough ($t_s \gg \tau_c$).

The variance Δ_x and Δ_y of the endpoints in the x and the y directions after the time t_s determines the diagonal components of the diffusion tensor by

$$D_{ii} = \frac{\Delta_i}{2t_s}, \quad i = x, y. \quad (6)$$

The criterion for Eq. (4) being valid is a linear relation between Δ and t . Figure 2 clearly demonstrates that this is fulfilled for the time range under study. For very short t , a deviation from linear spreading is observed because the trajectories do not start at a single point.¹⁸ The model was

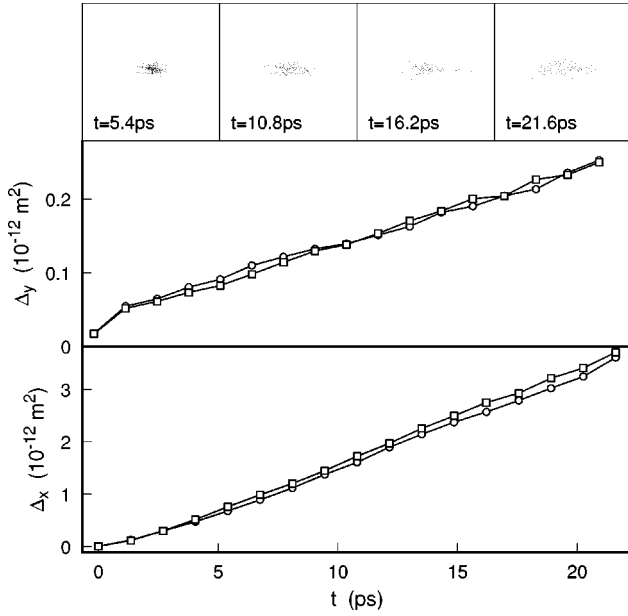


FIG. 2. Variance of the spreading cloud as a function of time (upper plot, y direction; lower plot, x direction), confirming that the model produces normal diffusion. The slight deviation from linear spreading at the beginning is due to initial condition (see text). The accuracy is demonstrated with the two different runs.

tested by calculating the conductivity σ_{ii} in the absence of antidots. The results match the values from the Drude formula within some percent.

IV. COMPARISON OF EXPERIMENTAL AND NUMERICAL DATA

The model contains three parameters to be estimated, namely, r , β , and τ_c . Their coarse values are known from the physical sample and only a fine tuning is performed by adjusting them to better fit the transport measurements. As an example, we take a measurement done with a positive gate voltage, resulting in a carrier density of $3.6 \times 10^{15} \text{ m}^{-2}$ ($E_F = 12.5 \text{ meV}$). From atomic force microscope pictures of the sample, the antidot radius can be estimated to $r \approx 0.2a_x$. The steepness can be estimated from the fact that an external potential should be screened out on a length scale of the screening length. Concerning Eq. (2), we use $\beta = 2$. In Fig. 1(b) the potential landscape is shown to give a visual impression. In Fig. 3 we show the experimental and the numerical curves for the longitudinal conductivities as a function of R_c . Note that R_c is inversely proportional to the magnetic field [Eq. (1)]. The conductivity along the rows of antidots (σ_{xx}) shows peaks when the cyclotron diameter is one or two times the smaller lattice constant a_x . The conductivity perpendicular to the antidot rows (σ_{yy}), shows weak minima at the corresponding positions.⁸ Between these positions of maximum anisotropy, the conductivity becomes nearly isotropic. The figure shows that the essential features are reproduced by the simulations. This proves that the commensurability oscillations are purely due to a modulation of the diffusion tensor. The modulation of the density of states that causes the Shubnikov–de Haas oscillations is not considered in this simulation. The conductivity along the antidot rows (σ_{xx}) is enhanced for commensurate magnetic fields

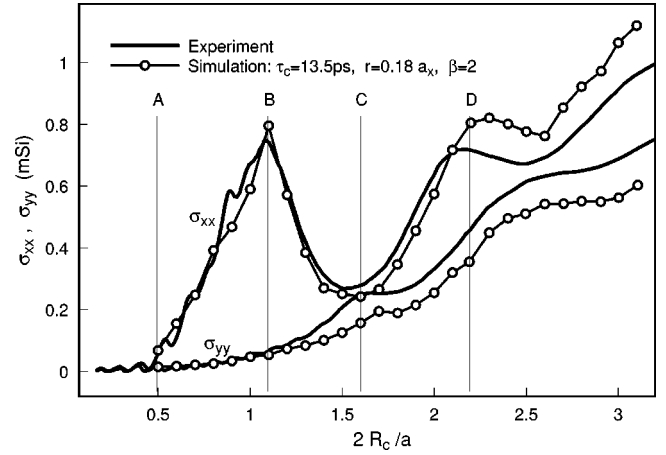


FIG. 3. Comparison of the experimental and numerical conductivity as a function of the cyclotron radius. The positions corresponding to the four pictures in Fig. 4 are indicated.

$2R_c = 1a_x, 2a_x$ (B, D) while the conductivity perpendicular to the antidot rows σ_{yy} is weakly reduced. For noncommensurate magnetic fields (e.g., $2R_c = 1.5a_x$) the conductivity is nearly isotropic (C). This behavior can be understood by studying the pictures of the trajectories as shown in Fig. 4. It can be seen how the trajectories are guided along the antidot rows in the case of commensurability (B, D) and how this effect lacks at noncommensurate fields (C). As already discussed in Ref. 9 we can confirm that it is mainly the enhanced diffusion along the antidot rows and not the pinning of orbits that leads to the commensurability oscillations observed in transport experiments. How important are the skipping and pinned orbits used to argue in earlier papers?^{3,7,9} Out of a large collection of pictures of trajectories, we found only a few that are skipping regularly from antidot to antidot for several periods, but a lot of them are diffusing in a chaotic way along the antidot rows and are pinned to them, because it is infrequent to skip from one row to the next without a scattering event. In this sense the trajectories are pinned and skipping at the same time.

Our simulation does not take into account that the scattering probability depends on the scattering angle and presum-

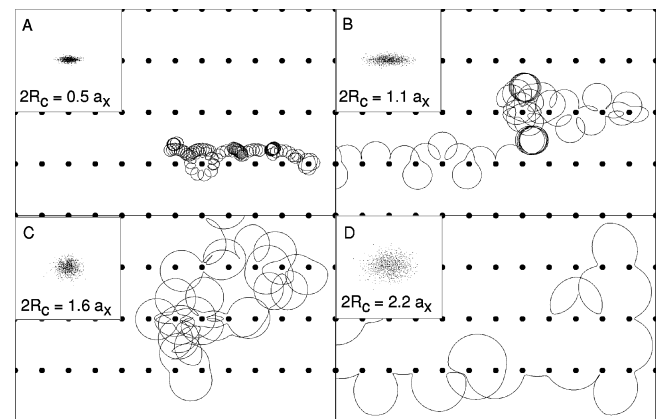


FIG. 4. The trajectories show how the anisotropic diffusion is originated. The inset shows the cloud of diffusing electrons ($t = 135 \text{ ps}$), which gets anisotropic for commensurate magnetic field (B, D) and nearly isotropic between (C).

ably on position. Furthermore, it neglects that the antidots are not circular. The anisotropy of the conductivity for zero magnetic field is much larger in the model than measured, probably due to noncircular antidots. It is anyway remarkable how this simple Drude-type model explains the magnetotransport in antidot arrays.

In conclusion, we have demonstrated that results of transport experiments on rectangular antidot arrays can be explained by a classical diffusion model and that all the parameters can be estimated realistically from physical considerations. Pictures of the diffusion clouds for different magnetic fields provide a intuitive visualization of the oscillatory behavior of the magnetoconductivity and of its anisotropy. Furthermore such illustrations clarify that it is mainly the enhanced diffusion along the antidot rows that is causing

the commensurability oscillations. Maps of trajectories in real space show how the anisotropic diffusion for commensurate magnetic fields is caused: the trajectories are following in a nonregular way the rows of antidots, rarely they skip from one row to the next. We expect that quantum effects get dominant as soon as the lattice constants gets in the range of the Fermi wavelength ($\lambda_F \approx 50$ nm). A quantum mechanical model of the diffusion in small antidot lattices can be performed in a similar way.

ACKNOWLEDGMENTS

The authors would like to thank R. Ketzmerick for valuable discussions. Financial support by the Schweizerischer Nationalfonds is gratefully acknowledged.

-
- ¹For a review, see R. Schuster and K. Ensslin, *Adv. Solid State Phys.* **34**, 195 (1994).
- ²K. Ensslin and P. M. Petroff, *Phys. Rev. B* **41**, 12 307 (1990).
- ³D. Weiss, M. L. Roukes, A. Menschig, P. Grambow, K. v. Klitzing, and G. Weinmann, *Phys. Rev. Lett.* **66**, 2790 (1991).
- ⁴A. Lorke, J. P. Kotthaus, and K. Ploog, *Superlattices Microstruct.* **9**, 103 (1991).
- ⁵R. Fleischmann, T. Geisel, and R. Ketzmerick, *Phys. Rev. Lett.* **68**, 1367 (1992).
- ⁶R. Kubo, *J. Phys. Soc. Jpn.* **12**, 570 (1957).
- ⁷E. M. Baskin, G. M. Gusev, Z. D. Kvon, A. G. Pogosov, and M. Entin, *Pis'ma Zh. Eksp. Teor. Fiz.* **55**, 649 (1992) [*JETP Lett.* **55**, 679 (1992)].
- ⁸R. Schuster, G. Ernst, K. Ensslin, M. Entin, M. Holland, G. Böhm, and W. Klein, *Phys. Rev. B* **50**, 8090 (1994).
- ⁹S. Lüthi, T. Vančura, K. Ensslin, R. Schuster, G. Böhm, and W. Klein, *Phys. Rev. B* **55**, 13 088 (1997).
- ¹⁰T. Nagao, *J. Phys. Soc. Jpn.* **64**, 4097 (1995).
- ¹¹T. Nagao, *J. Phys. Soc. Jpn.* **65**, 2606 (1996).
- ¹²K. Tsukagoshi, M. Haraguchi, K. Oto, S. Takaoka, K. Murase, and K. Gamo, *Jpn. J. Appl. Phys., Part 1* **34**, 4335 (1995).
- ¹³J. Takahara, A. Nomura, K. Gamo, S. Takaoka, K. Murase, and H. Ahmed, *Jpn. J. Appl. Phys., Part 1* **34**, 4325 (1995).
- ¹⁴R. Schuster, K. Ensslin, J. P. Kotthaus, M. Holland, and C. Stanley, *Phys. Rev. B* **47**, 6843 (1993).
- ¹⁵R. Schuster, K. Ensslin, J. P. Kotthaus, G. Böhm, and W. Klein, *Phys. Rev. B* **55**, 2237 (1997).
- ¹⁶K. Ensslin and R. Schuster, in *Fabrication and Electronic Properties of Antidot Superlattices*, edited by K. H. Ploog, III-V Quantum System Research (Institution of Electrical Engineers, United Kingdom, 1995), Chap. 4.
- ¹⁷K. Tsukagoshi, M. Haraguchi, S. Takaoka, and K. Murase, *J. Phys. Soc. Jpn.* **65**, 811 (1996).
- ¹⁸C. Jacoboni and L. Reggiani, *Rev. Mod. Phys.* **65**, 645 (1983).
- ¹⁹H. Silberbauer and U. Rössler, *Phys. Rev. B* **50**, 11 911 (1994); H. Silberbauer, P. Rotter, M. Suhrke, and U. Rössler, *Semicond. Sci. Technol.* **9**, 1906 (1994).
- ²⁰D. Weiss, K. Richter, A. Menschig, R. Bergmann, H. Schweizer, K. v. Klitzing, and G. Weinmann, *Phys. Rev. Lett.* **70**, 4118 (1993).